JOURNAL OF MATERIALS SCIENCE 22 (1987) 3652–3664

Phase relations and dielectric properties of $BaTiO_3$ ceramics heavily substituted with neodymium

T. R. N. KUTTY, P. MURUGARAJ
Materials Research Laboratory, Indian Institute of Science, Bangalore 560 012, India

Investigations on the phase relations and dielectric properties of $(1 - x)BaTiO_3 + xNd_{2/3}TiO_3$ (BNT) ceramics sintered in air below 1650 K have been carried out. X-ray powder diffraction studies indicate apparent phase singularity for compositions with $x < 0.3$. $Nd_2Ti_2O_7$ is detected at higher neodymium concentrations. The unit cell parameter changes continuously with neodymium content, and $BaTiO_3$ is completely cubic at room temperature with $x \simeq 0.0525$, whereas electron diffraction studies indicate that the air-sintered BNT ceramics with $x > 0.08$ contain additional phases that are partly amorphous even to an electron beam. SEM observations reveal that $BaTiO_3$ grains are mostly covered by a molten intergranular phase, and show the presence of randomly distributed $Nd_2Ti_2O_7$ grains. Energy dispersive X-ray analysis shows the Ba–Nd–Ti ternary composition of the intergranular phase. Differential thermal analysis studies support the formation of a partial melt involving dissolution–precipitation of boundary layers of $BaTiO_3$ grains. These complex phase relations are accounted for in terms of the phase instability of $BaTiO_3$ with large cation-vacancy concentration as a result of heavy Nd^{3+} substitution. The absence of structural intergrowth in $(1 - x)BaTiO_3 + xNd_{2/3}TiO_3$ under oxidative conditions leads to a separation of phases wherein the new phases undergo melting and remain X-ray amorphous. BNT ceramics with $0.1 < x < 0.3$ have $\varepsilon_{eff} \gtrsim 10^4$ with $\tan \delta < 0.1$ and nearly flat temperature capacitance characteristics. The grain-size dependence of ε_{eff}, variations of ε_{eff} and $\tan \delta$ with the measuring frequency, the non-ohmic resistivities, and the non-linear leakage currents at higher field-strengths which are accompanied by the decrease in ε_{eff} and rise in $\tan \delta$, are explained on the basis of an intergranular (internal boundary layer) dielectric characteristic of these ceramics.

1. Introduction

The electrical resistivity of donor-doped $BaTiO_3$ ceramics does not decrease proportionally with the donor concentration [1–3]. For example, $BaTiO_3$ ceramics doped with less than 0.5 at % Nd are semiconducting even when sintered in air. If the cooling rate is slow (10 to 20 K h^{-1}), the same ceramics are insulating with effective dielectric constant $\varepsilon_{eff} > 10^5$ and are known as the grain-boundary layer capacitor (GBLC) ceramics [1, 4–6]. The high ε_{eff}, in this case is due to their microstructure, in which the grain-boundary layers are insulating and the grain interiors are semiconducting [5, 6]. At levels above 0.5 at % Nd and with air as the sintering atmosphere, $BaTiO_3$ ceramics are light-coloured and completely insulating, independent of the cooling rate. The value of ε_{eff} at room temperature decreases with neodymium content. ε_{eff} goes through a minimum at ~2.0 at % Nd and is enhanced to $\sim 10^4$ at higher concentrations. The diffuse phase transformation (DPT) behaviour of these compositions has been reported earlier [7]. Since $BaTiO_3$ with more than 3.6 at % Nd consists predominantly of the para-electric cubic phase at room temperature, the enhanced ε_{eff} is indicative of an intergranular boundary layer effect. As the donor content is increased, the Curie point shifts to a lower temperature and is accompanied by a reduction in grain size to $\leqslant 1\ \mu m$ [8, 9]. Higher sinter density is usually obtainable for these ceramics only above 1675 K. The present observations show that the sintering temperature can be lowered to ~1500 K when the neodymium content is above 7.5 at %, provided an appropriate amount of TiO_2 is added for compositional adjustment. The resulting ceramics showed nearly flat temperature capacitance characteristics at 200 to 400 K with $\varepsilon_{eff} \sim 10^4$ and loss tangents of less than 0.1. Because of the continued interest in temperature-stable dielectric ceramics with lower firing temperatures, we undertook these investigations on $(1 - x)BaTiO_3 + xNd_{2/3}TiO_3$ compositions (designated as BNT ceramics).

The phase relations in $BaTiO_3$ containing larger concentrations of lanthanides are not well established. Eror and Smyth [10] have reported that $BaTiO_3$ containing up to 20 at % La retains phase singularity even in fully oxidized samples. This may correspond to the composition $Ba^{2+}_{0.8}La^{3+}_{0.2}Ti^{4+}O_{3.1}$. It is not certain how the extra oxygen in the perovskite lattice is accommodated. It was proposed that a superlattice accommodation of excess "BaO" in the perovskite phase is

0022–2461/87 $03.00 + .12

possible which involves a crystallographic shear mechanism, analogous to the $SrO-nSrTiO_3$ phases described by Ruddlesden and Popper [11]. This comparison sounded reasonable since (Sr, La)TiO_3 with 40 at % La is reported to be homogeneous [12]. Earlier, Tien and Hummel [13] have reported ordering in a $SrO-TiO_2-La_2O_3$ ternary system containing 70 mol % $La_{2/3}TiO_3$ in $SrTiO_3$. Although pure $La_{2/3}\square_{1/3}TiO_3$, where $\square$ represents the vacant cation site, cannot be prepared, small quantities of $SrTiO_3$ or $PbTiO_3$ are said to stabilize this phase [14]. On the other hand, Tofield [15] observed that the range of solubility for lanthanum in $SrTiO_3$ is limited in an oxidizing atmosphere. A more recent article has shown the absence of Ruddlesden–Popper type superlattice ordering of BaO in $BaTiO_3$ [16]. Thus, the problem of accommodating excess oxygen in air-sintered (Ba, Ln)TiO_3 (Ln = lanthanides) remains unexplained, and a closer scrutiny of the phase relations with techniques more sensitive than X-ray powder diffraction is necessary. The present electron diffraction (ED) studies have indicated phase inhomogeneity in $Ba_{1-x}Nd_xTiO_3$ ceramics with $x \gtrsim 0.1$. The nature of the coexisting phases in the $BaO-Nd_2O_3-TiO_2$ quasi-ternary system, heated in air at $\leqslant 1650$ K, is presented in this paper.

2. Experimental procedure

$BaTiO_3$ with low background impurities (Mn < 0.1, Fe < 1.0 $\mu g\,g^{-1}$) was prepared from successively precipitated precursor oxalate, $BaTiO(C_2O_4)_2 \cdot 4H_2O$. Samples containing higher neodymium concentrations were prepared by the coprecipitation of oxalates. The products resulting from the thermal decomposition of these oxalates at 1100 K were adjusted with TiO_2 so that the final compositions were in accordance with the formula $(1-x)BaTiO_3 + xNd_{2/3}TiO_3$ which followed the corresponding tie-line in the three-component diagram (Fig. 1). These powders were precalcined for 3 h at 1350 K. Discs of 10 mm diameter and 1 mm thickness were then sintered in air for 3 to 8 h at 1450 to 1650 K. The samples were cooled to room temperature at a rate of 100 K h^{-1}, resulting in non-porous ceramics as shown from the SEM studies. The sinter densities of low x-value compositions were 97 to 99%. Polishing the discs with rough emery (1/0) followed by fine emery (4/0) paper was commonly adopted to remove the surface layers so as to ensure that the measured electrical properties were of the bulk rather than those of the surfaces. For the electric measurements, electroless nickel was deposited on the discs followed by nickel-electroplating and annealing at 550 K to yield good ohmic contacts. The ε_{eff} values were measured using a bridge having a separate oscillator and a detector at 4 $V_{r.m.s.}\,mm^{-1}$ field strength. The temperature of the sample was slowly varied from 150 to 450 K at a rate of 2 K min^{-1}. The X-ray investigations were carried out with a Philips 1700 powder diffractometer, using nickel-filtered Cu$K\alpha$ radiation. Transmission electron microscope studies were carried out with a Philips TEM 301. Powder mounting of the fragmented ceramics on a carbon film deposited on a copper grid was used for obtaining the electron diffraction patterns. Although more laborious, this method was free of any possible artefacts introduced during specimen thinning by ion-milling. Evaporated gold film was used for the calibration of d-spacings. Differential thermal analysis (DTA) experiments were conducted with a Stanton–Redcroft equipment (Pittsburgh, Pennslyvania). SEM photographs of the sintered discs were obtained from a Cambridge Stereoscan 150. This instrument was fitted with an EDAX-711 energy-dispersive X-ray analyser for the elemental analysis (EDAX) of individual grains in the ceramics.

3. Results

3.1. X-ray powder diffraction

Fig. 2a shows the variations in cell parameters of $BaTiO_3$ at room temperature with increase in neodymium content. For the undoped $BaTiO_3$ (tetragonal) the cell parameters are $a_0 = 0.3991$ and $c_0 = 0.4037$ nm. On enhancing the x-value, a_0 increases whereas c_0 decreases and at $x \simeq 0.0525$, the phase becomes completely cubic with $a_0 = 0.4006$ nm. The lattice parameter a_0 decreases at higher x-values and attains constancy at $x \simeq 0.2$ with $a_0 = 0.3997$ nm. Broadening of the diffraction peaks is observed in the further range $0 < x < 0.0525$. There is no further line-broadening at higher x-values, as exemplified in Fig. 2b by the peak-width at half

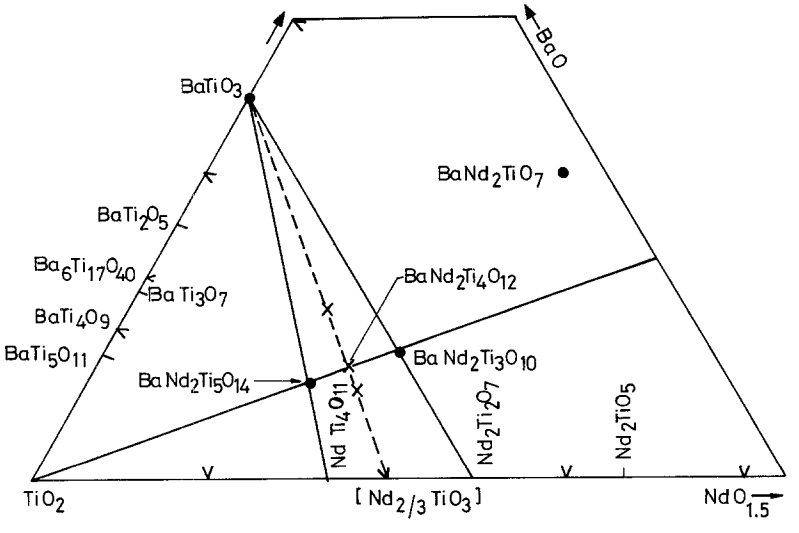

Figure 1 Part of the ternary diagram of the $BaO-Nad_2O_3-TiO_2$ system showing various compounds reported. The dashed line indicates the range of compositions of the present investigation.

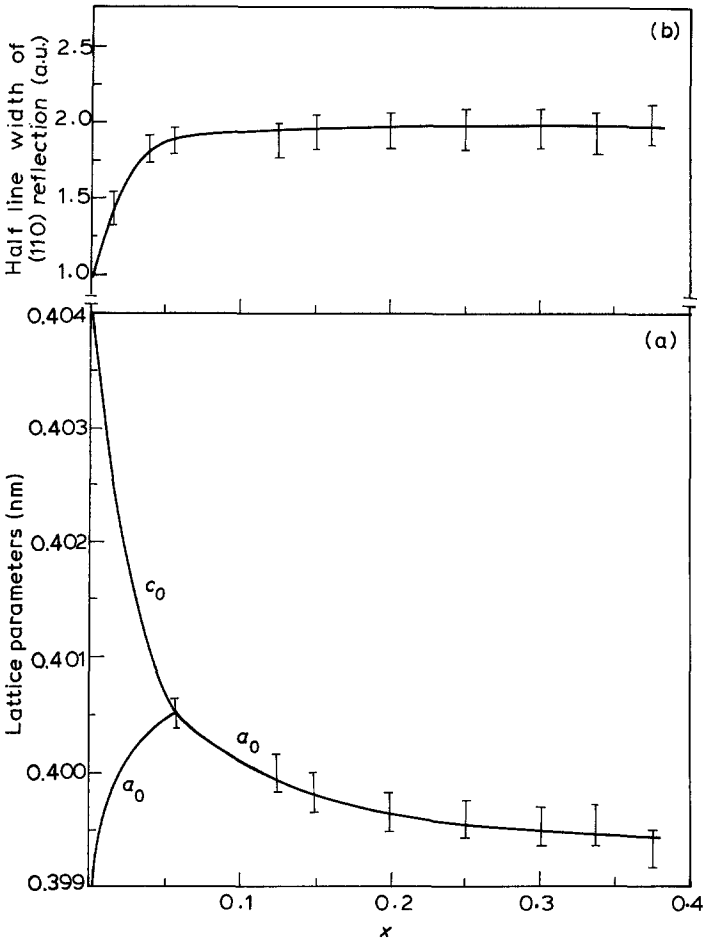

Figure 2 (a) The variation of lattice parameters (a_0 and c_0) with the value of x in the $(1 - x)BaTiO_3 + xNd_{2/3}TiO_3$ system. (b) The variation of peak width at half maximum of the X-ray reflection (d_{110}) for $(1 - x)BaTiO_3 + xNd_{2/3}TiO_3$.

maximum of (1 1 0) reflection, whereas the intensities of the diffraction peaks obtained under the same experimental conditions decrease when $x > 0.075$. When $x > 0.3$, the X-ray powder diffractograms show additional reflections which do not arise from the cubic perovskite lattice (Fig. 3). These extra peaks gain intensity as the x-value is enhanced. The additional reflections may arise from any compound in BaO–TiO_2, Nd_2O_3–TiO_2 or BaO–Nd_2O_3–TiO_2 systems. Comparisons with the reported X-ray data of the various compounds in these systems indicate that the additional reflections arise from $Nd_2Ti_2O_7$. This was further confirmed by preparing $Nd_2Ti_2O_7$ by annealing $Nd_2O_3 + 2TiO_2$ at 1500 K for 12 h (Fig. 3). The $Nd_2Ti_2O_7$ is monoclinic with space group $P2_1$ and is isomorphous with $La_2Ti_2O_7$ [17]. The corresponding reflections in the neodymium-substituted $BaTiO_3$ ceramics are shifted to lower 2θ values, possibly due to the incorporation of Ba^{2+} in $Nd_2Ti_2O_7$. In order to study the effect of barium substitution, $Nd_2Ti_2O_7$ with various amounts of BaO ($\lesssim 10$ wt %) were prepared. The d-values of $Nd_2Ti_2O_7$ increase with BaO content as illustrated by the change in $d_{(1\,1\,2)}$ spacing as a function of BaO concentration (Fig. 4a). Correspondingly, the lattice constants of $Nd_2Ti_2O_7$ change from $a_0 = 1.308$, $b_0 = 0.548$ and $c_0 = 0.768$ nm to 1.308, 0.551 and 0.771 nm, respectively, with $\beta = 98.5°$ remaining nearly unchanged. The intensities of $Nd_2Ti_2O_7$ X-ray reflections decrease with BaO content.

Cubic $BaTiO_3$ (containing $x \simeq 0.06$ $Nd_{2/3}TiO_3$) and $Nd_2Ti_2O_7$ were mechanically mixed in different ratios. The intensities of (1 1 0) and (1 1 2) reflections from $BaTiO_3$ and $Nd_2Ti_2O_7$, respectively, were measured for sintered ceramics of the same composition (Fig. 4b). Similar results were obtained in neodymium-rich compositions as well. These results indicate the formation of X-ray amorphous phases during the sintering of $(1 - x)BaTiO_3 + xNd_{2/3}TiO_3$ ceramics. Possibly these phases can be characterized only by techniques more sensitive than X-ray diffraction. Throughout the compositional range of the present investigation, no X-ray reflection from $BaNd_2Ti_5O_{14}$ could be identified. This compound has been reported by Kolar *et al.* [18] in the ternary BaO–Nd_2O_3–TiO_2 system. Similarly, no $BaTi_nO_{2n+1}$ where $n = 2, 3, 4, \ldots$ could be detected [19, 20].

3.2. Electron diffraction studies

Electron diffraction (ED) patterns of BNT ceramics with $x < 0.075$ show no phases other than cubic $BaTiO_3$. Both mono- and poly-crystalline patterns are observed (Fig. 5). Samples with $0.075 < x < 0.15$ show diffraction patterns from two distinct crystalline phases – one corresponding to cubic $BaTiO_3$ and the other to $Nd_2Ti_2O_7$ – as identified by their d-values. Additionally a few of the ED photographs showed broader diffraction rings (Fig. 5b). With $0.15 < x < 0.225$, the frequency of appearance of the pattern in Fig. 5b increases. A monocrystalline patterns of $Nd_2Ti_2O_7$ as in Fig. 5c is less frequently observed and is often superimposed on the extremely broad diffraction rings typical of the amorphous phase. In BNT ceramics with $x > 0.225$, single- crystalline $Nd_2Ti_2O_7$ patterns appear more often and so also do the

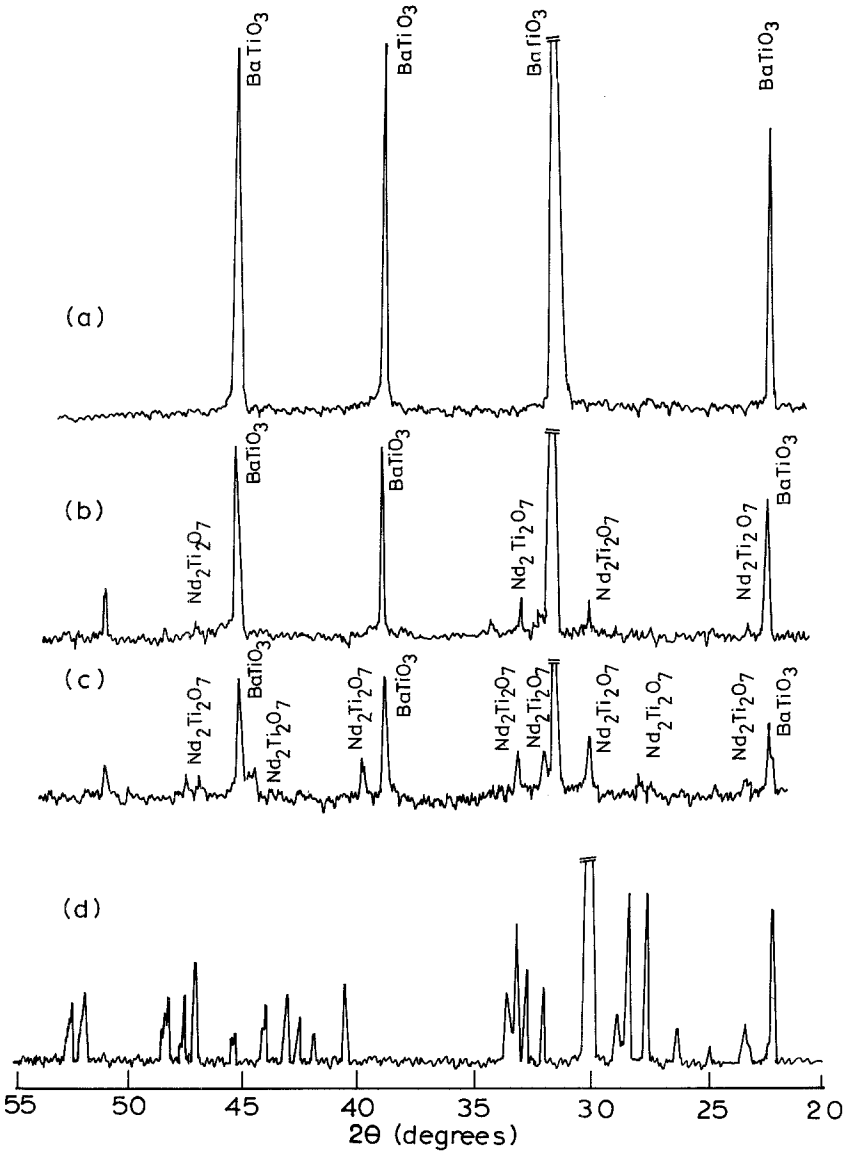

Figure 3 X-ray diffraction traces of $(1 - x)BaTiO_3 + xNd_{2/3}TiO_3$ system: (a) $x = 0.053$; (b) $x = 0.3$ and (c) $x = 0.5$; (d) is for $Nd_2Ti_2O_7$.

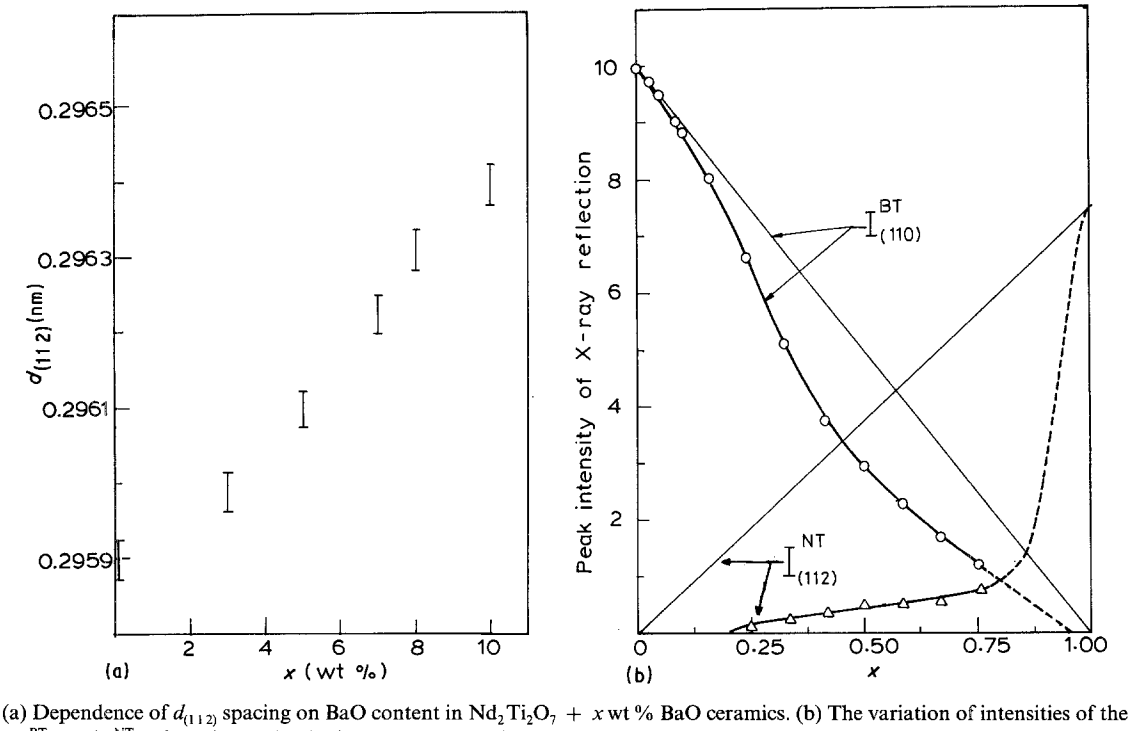

Figure 4 (a) Dependence of $d_{(112)}$ spacing on BaO content in $Nd_2Ti_2O_7 + x$ wt % BaO ceramics. (b) The variation of intensities of the X-ray reflections $I^{BT}_{(110)}$ and $I^{NT}_{(112)}$ of $BaTiO_3$ and $Nd_2Ti_2O_7$, respectively, in $(1 - x)BaTiO_3 + xNd_{2/3}TiO_3$. Solid lines are for the mechanical mixture of $BaTiO_3$–$Nd_2Ti_2O_7$, while the broken lines represent corresponding intensity variations in the sintered sample.

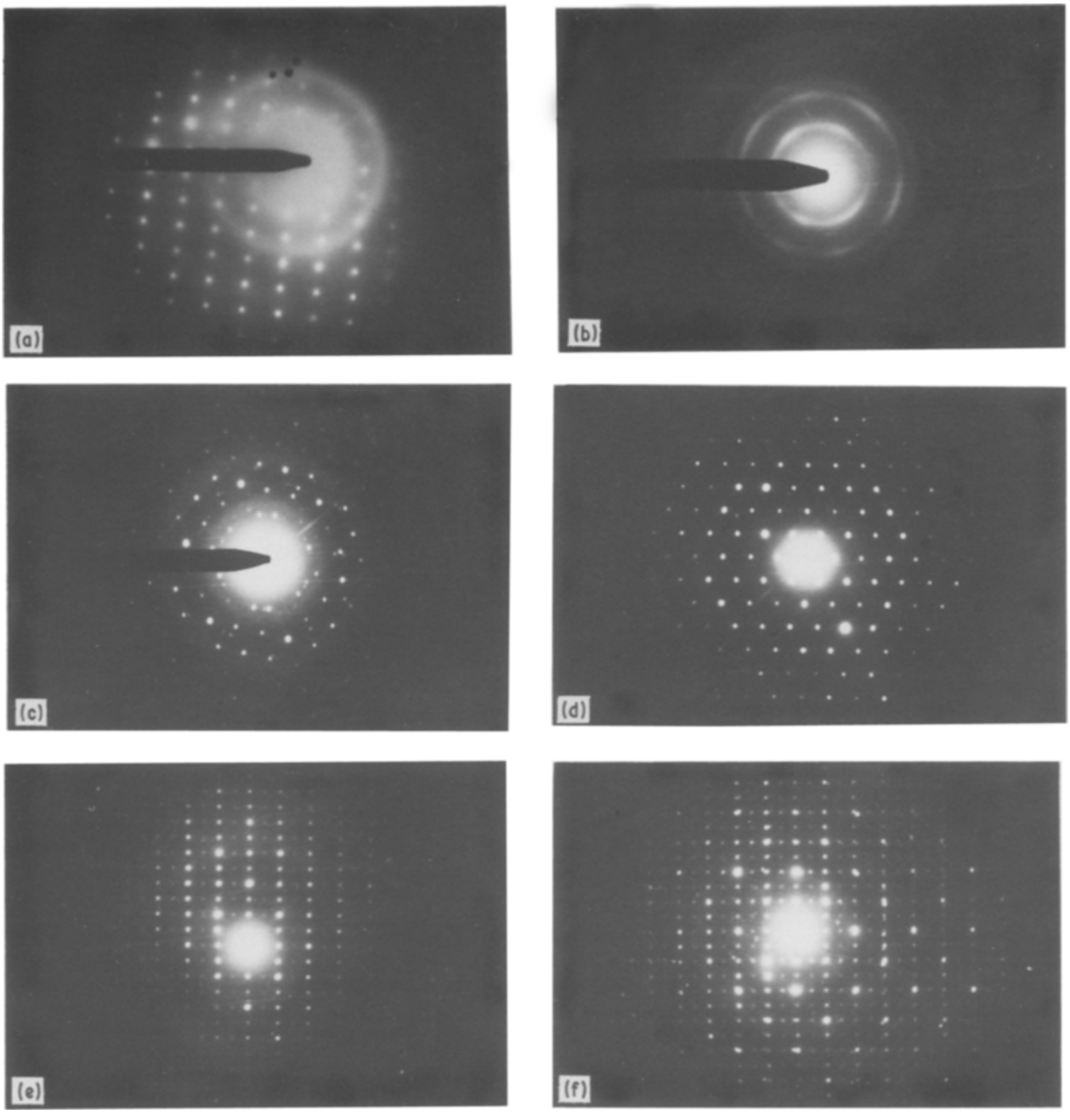

Figure 5 Electron diffraction patterns of $(1 - x)BaTiO_3 + xNd_{2/3}TiO_3$ compositions. (a) Monocrystalline pattern of cubic $BaTiO_3$; (b) typical powder pattern obtained in the compositions with $x = 0.1$; (c) patterns observed for samples with $x = 0.2$; (d) monocrystalline pattern of $Nd_2Ti_2O_7$ observed in ceramics with $x = 0.45$; (e, f) sample with $x = 0.45$ annealed in air for over 8 h at 1600 K.

polycrystalline diffraction rings of $BaTiO_3$. On a statistical average, only one out of every fifteen fragments examined showed spotty ED patterns of $BaTiO_3$. In ceramics with $x > 0.3$, monocrystalline ED patterns of $Nd_2Ti_2O_7$ appear more often. For the ceramics with $x > 0.4$ annealed in air for over 8 h near the sintering temperature, ED patterns as in Fig. 5e and f are additionally observed. These photographs show the superlattice ordering. However, we have not identified the corresponding phase.

Thus the electron diffraction studies indicate that the air-sintered BNT ceramics with $0.075 < x < 0.225$ contain additional phases, other than $BaTiO_3$, that are partly or fully crystalline to the electron beam although X-ray diffraction showed apparent phase singularity.

3.3 SEM and EDAX results

Fig. 6 shows SEM photographs of the fractured and thermally etched surfaces. The average grain size decreases with neodymium content as is evident from Figs 6a and b. At higher neodymium contents ($x > 0.02$), the grain size remains nearly the same (0.5 to 3 μm). The needle-shaped $Nd_2Ti_2O_7$ can be clearly distinguished from the nearly rounded $BaTiO_3$ grains for ceramics of $x > 0.3$ (Fig. 6c). The needle-shaped phase increases with further enhancement of neodymium content. In the compositional range $0.075 < x < 0.3$ $BaTiO_3$ grains are seen enveloped by a second phase, particularly when the sintering temperature is increased from 1500 to 1600 K (Fig. 6d) and also when the sintering time is extended from 3 to 8 h (Fig. 6e). With higher temperature and longer durations of

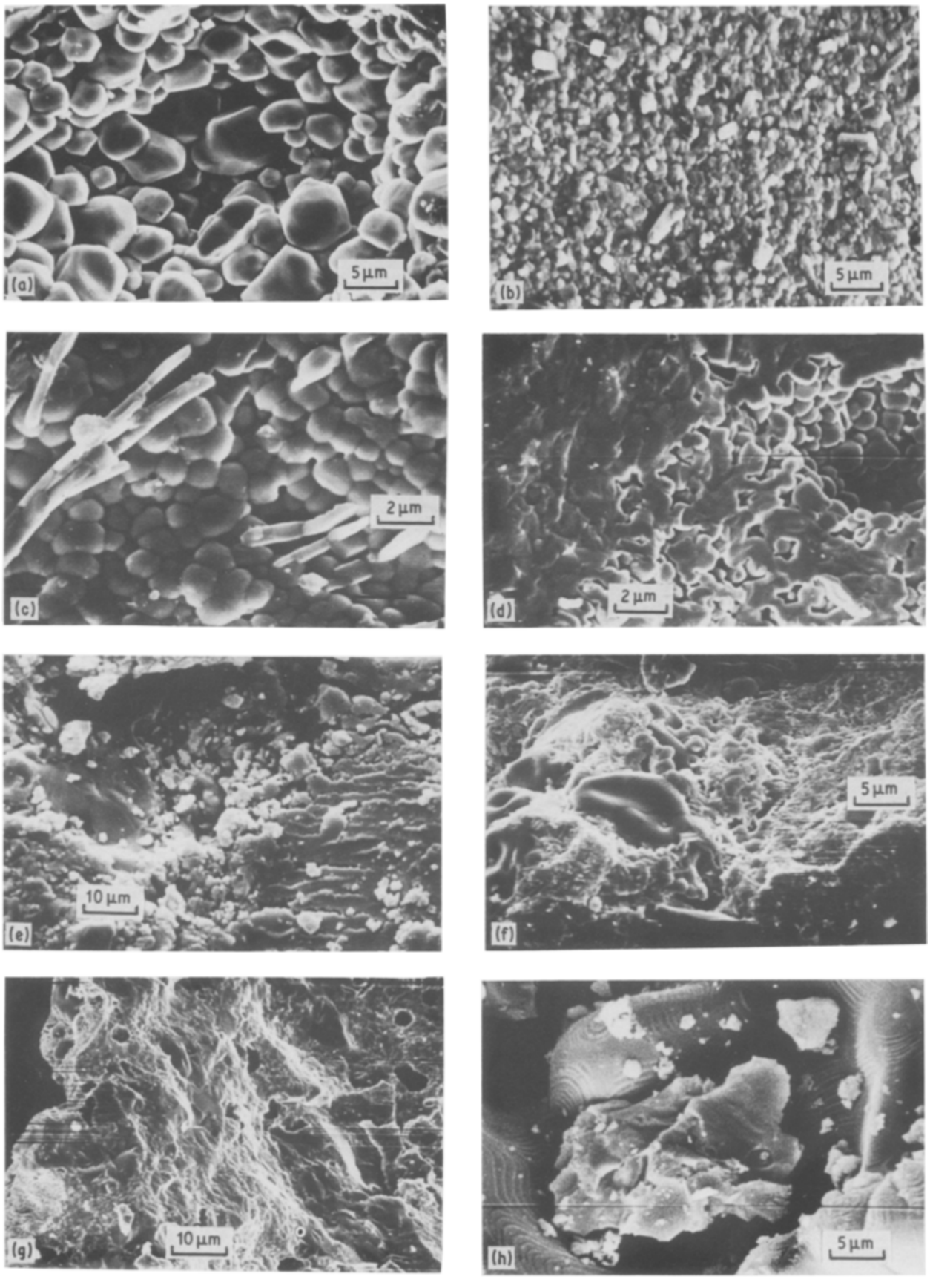

Figure 6 SEM micrographs of the fractured surfaces of $(1 - x)BaTiO_3 + xNd_{2/3}TiO_3$ ceramics. (a) $x = 0.001$; (b) $x = 0.01$; (c) $x = 0.35$; (d) $x = 0.35$ (sintered at 1600 K for 3 h); (e) $x = 0.25$ (sintered at 1550 K for 8 h); (f) $x = 0.25$ when the degree of melting is increased; (g) $x = 0.25$ with high amount of molten phase present, showing concoidal fracturing, and (h) magnified micrograph of the same surface showing solidification fronts.

sintering, the second phase exhibits all the characteristics of a melt subsequently solidified. Fig. 6f shows that the fractures have mostly occurred along the grain boundaries so that some of the depressions are parted grain-boundary surfaces. In the case of samples with a higher degree of melting, concoidal fracturing with the sharper edges characteristic of glassy materials is observed (Fig. 6g). In this figure, the depressions

indicate the parted grain-boundary surfaces and they are not rounded. These observations may indicate partial dissolution of the $BaTiO_3$ grains to give rise to the glassy phase. Under higher magnification the fracture surfaces of such samples show lines which are the solidification fronts of a molten phase (Fig. 6h). Thus, the microstructural observations on BNT ceramics reveal three phases: $BaTiO_3$ grains, intergranular material and a randomly distributed second phase.

In order to identify the compositional differences, if any, between the above three phases, the EDAX results have been somewhat useful. Due to the close energy value of Ba$L(\alpha$ and $\beta)$ and Ti$K\alpha$ spectral lines, the concentrations of barium could not be estimated with certainty, whereas the neodymium contents can be evaluated from the intensities of Nd$L\beta$ and Nd$M(\alpha$ and $\beta)$. The relative intensities of neodymium spectral lines are enhanced in the order: $BaTiO_3$ grains < intergranular material < second phase. The asymmetry of the X-ray spectral lines around 4.5 keV indicates that the relative variations of barium content may be in the reverse order. Considering the X-ray diffraction and ED results, the second phase may therefore correspond to $Nd_2Ti_2O_7$ and the intergranular material is likely the X-ray amorphous phase of ternary compositions. The fact that neodymium lines of lower intensities are seen for the $BaTiO_3$ grains is explainable in terms of the incorporation of neodymium in $BaTiO_3$.

3.4. Differential thermal analysis

The presence of an X-ray amorphous intergranular phase is indicative of the formation of a liquid phase during sintering and its possible involvement in densification. DTA of the BNT compositions was therefore undertaken. The initial DTA run of the powder with $x = 0.25$ shows a broad endothermic peak around 1570 K and on cooling a shallow exotherm around 1480 K (Fig. 7). On re-running the DTA of the same sample, these thermal effects are shifted to somewhat lower temperature accompanied by enhanced intensities. A reversal in the temperature shift of the DTA peaks is noticed as the number of DTA cycles is increased, accompanied by diminishing peak heights, and finally the thermal effects are barely discernible. These results can be explained on the basis of the progressive formation of the melt in the early DTA cycles. During the later cycles the melting temperature is enhanced, together with the gradual disappearance of the melt. The DTA results also indicate that only a part of the BNT compositions form the molten phase which may involve the dissolution of smaller $BaTiO_3$ grains. On the other hand, the boundary regions of the larger grains may undergo a dissolution–precipitation process so that the melting temperature is enhanced and the melt disappears as the sintering advances. SEM observations also support the same conclusion.

3.5. Dielectric measurements

Fig. 8 shows the variation of ε_{eff} with neodymium content at 1 kHz and 300 K for ceramics sintered in air and cooled at 20 to 30 K h^{-1}. The dielectric properties of the ceramic with $x > 0.065$ have been reported in previous publications [6, 7]. The large ε_{eff}(max) at $x \simeq 0.0075$ is due to the GBLC behaviour [4, 6]. When cooled at faster rates (75 to 150 K h^{-1}) after sintering, the ceramics of these compositions have low resistivities (10 to 100 Ω cm) and exhibit a positive temperature coefficient in resistivity (PTCR) around T_C. The second maximum in Fig. 8 at $x \simeq 0.06$ arises from the shift in T_C to lower temperatures with neodymium content which is associated with the diffuse phase transformation of the system [7]. The third maximum in ε_{eff} is broad and prevails over a wider compositional range of $0.12 < x < 0.3$ (Fig. 8). The value of ε_{eff} is $\geqslant 10^4$ and is only marginally altered by the various sintering parameters such as the surrounding atmosphere (p_{O_2} ranging from 2×10^{-1} to 1×10^{-6} atm), temperature, and the cooling rates. Fig. 8 also depicts the change in grain size with composition. Large grain size is difficult to achieve in BNT ceramics with $x > 0.03$ even when the (Ba + Nd)/Ti

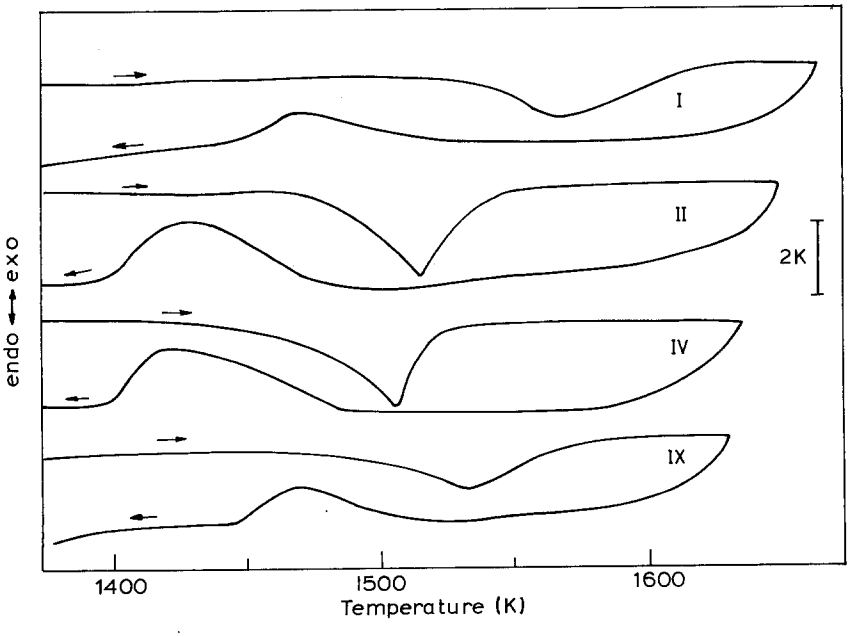

Figure 7 DTA traces obtained for $(1 - x)BaTiO_3 + xNd_{2/3}TiO_3$ ceramics. The number on each curve indicates the number of heating and cooling cycles.

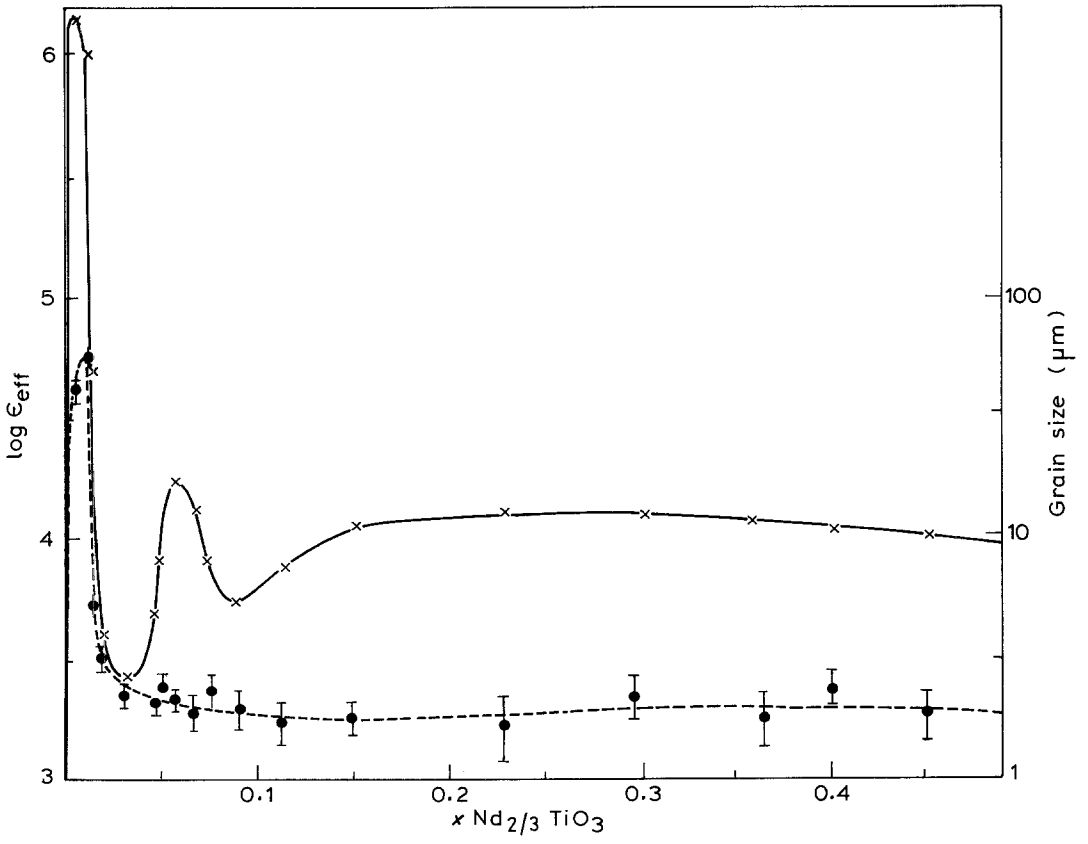

Figure 8 The variation of (×) ε_{eff} at 1 kHz, 300 K and (●) average grain size of $(1 - x)BaTiO_3 + xNd_{2/3}TiO_3$ ceramics with x-values.

ratio, heating schedules and atmosphere of sintering are varied. However, at faster heating rates (100 to 200 K h^{-1}) in the range of 1350 to 1500 K, the average grain size can be brought down to 0.25 μm for ceramics with $x = 0.15$ to 0.35. Such samples have lower ε_{eff} values. Ceramic discs of different thickness but of the same composition show nearly similar ε_{eff} values, indicating that ε_{eff} is a bulk rather than a surface property which may arise from the non-ohmic metal electrode–ceramic contacts.

The BNT ceramic with $x = 0.075$ has ε_{eff}(max) around 250 K which corresponds to the Curie point (Fig. 9). T_C is further lowered with x-value so that only the descending parts of the ε_{eff}–T curve can be observed in the measuring range of 150 to 480 K for ceramics with $x > 0.12$. The temperature coefficient of ε_{eff} is very low for specimens with $x > 0.2$ and the magnitude of ε_{eff} is $\geqslant 10^4$. The tan δ values are lower than 0.1 and increase continuously with temperature. Fig. 10 shows that ε_{eff} decreases with frequency and above 1 MHz the values drop perceptibly. The lowest frequency dispersion is noticed for ceramics with $0.15 < x < 0.25$. The tan δ values are minimum around 10 kHz. ε_{eff} decreases at high field strengths of measurement which correspond to those around which the d.c. resistivities fall (see Section 3.6).

Low frequency (< 1 kHz) measurements of ε_{eff} and tan δ values show some interesting features. At 50 Hz, ε_{eff} of samples with $x = 0.075$ has a maximum around 250 K (T_C), and above 370 K a further increase is noticed. The upward trend persists beyond the present measuring range (Fig. 11). At 100 Hz, the value of ε_{eff} below 370 K remains unchanged with temperature, whereas the temperature coefficient above 370 K is enhanced. It is evident from Fig. 11 that the temperature dependence of tan δ has a maximum which

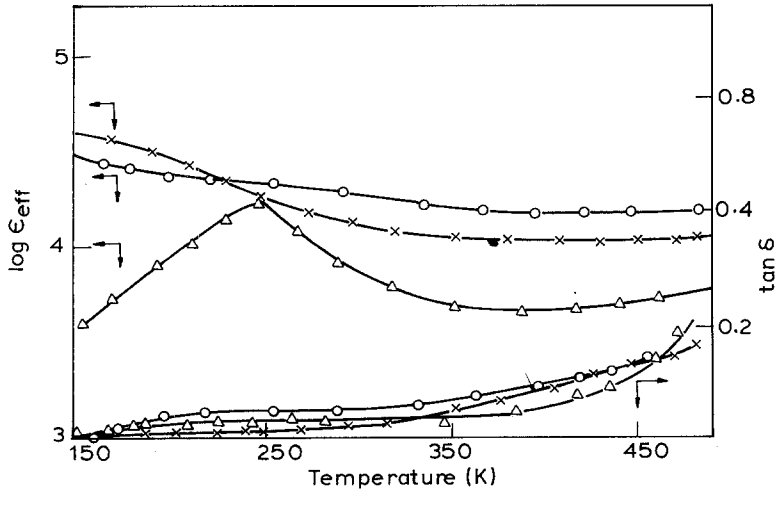

Figure 9 The variation of ε_{eff} and tan δ at 1 kHz with temperature for $(1 - x)$ $BaTiO_3 + xNd_{2/3}TiO_3$ ceramics. (△) $x = 0.075$, (×) $x = 0.15$, (○) 0.3.

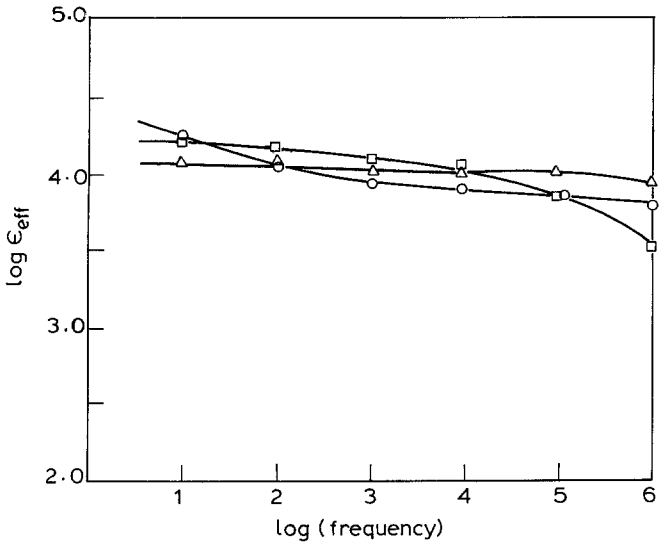

Figure 10 Frequency dependence of ε_{eff} for $(1 - x)$ $BaTiO_3$ + $xNd_{2/3}TiO_3$ ceramics. (○) $x = 0.15$, (×) $x = 0.225$, (△) $x = 0.3$.

shifts to higher temperature with the applied frequency. The anomalous changes in ε_{eff} and tan δ are not observed at frequencies above 5 kHz. Samples with $x = 0.15$ also show similar trends except that the whole set of curves shifts to lower temperatures (Fig. 12). The maxima on the tan δ–T curves decrease with x-value and disappear for samples with $x > 0.25$. The frequency dependences of ε_{eff} and tan δ are not very different for ceramics sintered and cooled in nitrogen as compared to those processed in air. In general, the frequency dispersions at higher measuring temperatures are slightly smaller for ceramics cooled in nitrogen.

In order to study the influence of a reducing atmosphere during sintering, ceramics with $x = 0.2$ to 0.35 were sintered in N_2–H_2 (80%:20%) at 1500 K. The resistivities of these samples were 5 to 30 Ω cm. They were re-equilibrated in air at 1300 K, whereupon they remained still conductive ($< 10^3$ Ω cm).

3.6. Effect of field strength on resistivity

The d.c. resistivities of BNT ceramics vary non-linearly with increasing field strength. The resistivity decreases at higher field strength when the composition is increased from $x = 0.075$ to 0.3 (Fig. 13). The voltage-withstanding capability of the ceramics will also depend on the cooling rate and annealing conditions. The non-ohmic resistivity variations generally follow the relation

$$\varrho = \varrho_0 E^{-\alpha} \quad (1)$$

where ϱ_0 is the resistivity at unit field strength, E is the applied field strength and α is a constant, the value of which ranges from 2.5 to 4.5. The samples annealed in nitrogen show a decrease in resistivity at lower E values. The change in capacitance up to the field strength where the leakage current starts increasing is negligible. The decrease in ε_{eff} at higher applied fields is accompanied by a rise in the loss tangent.

4. Discussion

Since $BaTiO_3$ doped with less than 0.5 at % Nd is highly conducting, it is generally accepted that Nd^{3+} acts as a donor by replacing Ba^{2+} in the $BaTiO_3$ lattice. By definition, an impurity cation that has a higher valence than that of the host cation that it replaces is called a donor. The effective positive charge on these impurity centres can be compensated by an electron in the conduction band, a cation vacancy or an acceptor impurity. In $BaTiO_3$, the conduction band

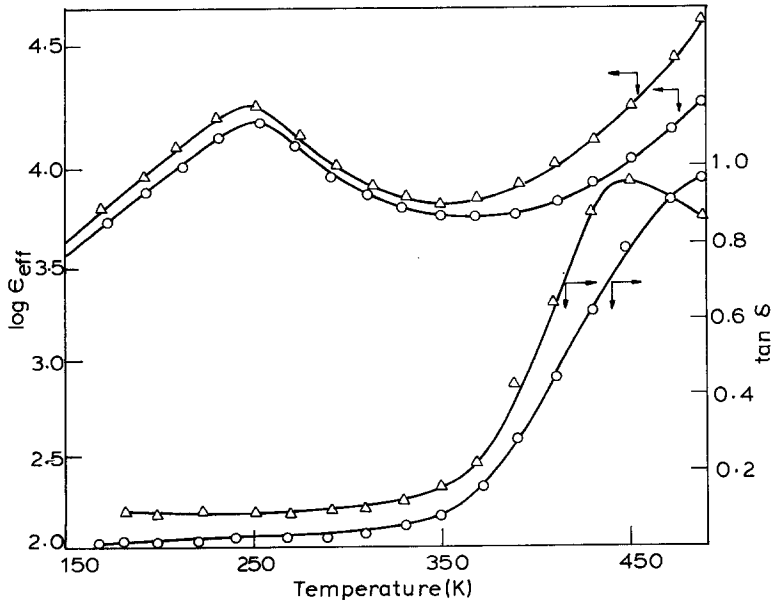

Figure 11 ε_{eff} and tan δ against temperature for $(1 - x)BaTiO_3$ + $xNd_{2/3}TiO_3$ ceramic ($x = 0.075$) at various frequencies: (△) 50 Hz, (○) 100 Hz.

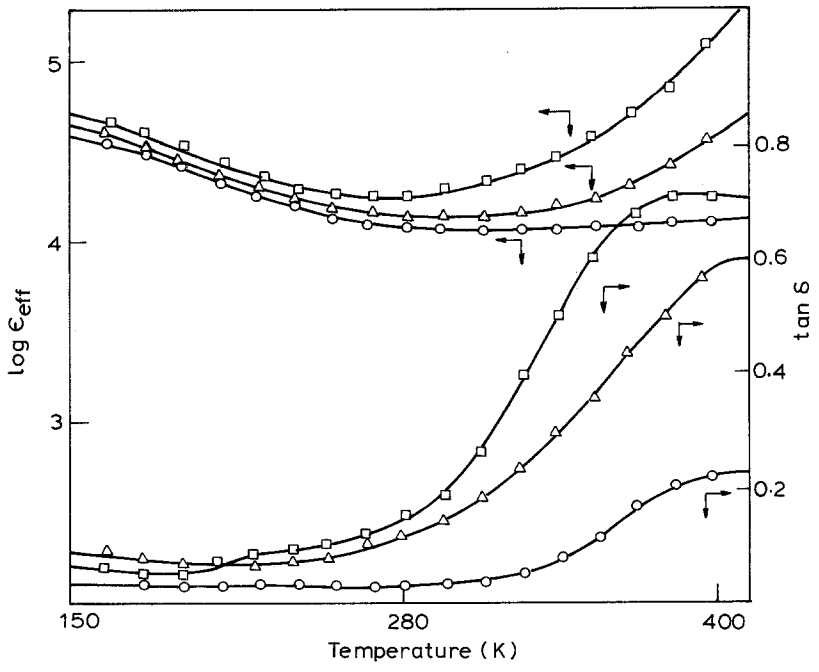

Figure 12 ε_{eff} and tan δ at 1 kHz against temperature for $(1 - x)BaTiO_3 + xNd_{2/3}TiO_3$ ceramic ($x = 0.15$) at various frequencies: (□) 50 Hz, (△) 100 Hz, (○) 1 kHz.

is mostly constituted from the empty 3d orbitals of Ti^{4+} ions, so that the electron compensation of the donor can be represented as

$$Ba^{2+}_{1-x}Nd^{3+}_{x}Ti^{4+}_{1-x}Ti^{3+}_{x}O_3 \qquad (2)$$

A vacancy compensation of the mixed type has to be considered if the results from the weight-loss experiments [10] and the electron paramagnetic resonance spectra [21, 22] are also taken into account:

$$(Ba^{2+}_{1-3x}Nd^{3+}_{2x}\square^{Ba}_{x})(Ti^{4+}_{1-2x}Ti^{3+}_{2x})O_{3-x}(V_O)_x \qquad (3)$$

where barium vacancies, Ti^{3+} and oxygen vacancies (V_O) are generated by the mixed mode of compensation. Both Ti^{3+} as well as the ionization of neutral V_O render the material conducting. Electron paramagnetic resonance (EPR) investigations have shown that parts of Ti^{3+} and V_O are associated so as to form Ti^{3+}–V_O defect complexes [21]. These studies have also shown the presence of singly ionized barium vacancies (V'_{Ba}) in cubic $BaTiO_3$ above T_C.

At $x > 0.075$ the resistivity of $BaTiO_3$ ceramics starts increasing with neodymium content, which may be due to more than one reason. There may be changes in the compensation mechanism for Nd^{3+} at higher concentration levels wherein cation vacancy compensation is predominant. If Nd^{3+} substitution is assumed to be restricted to the barium sublattice, then the following type of substitution is possible:

$$(Ba^{2+}_{1-x}Nd^{3+}_{2x/3}\square^{Ba}_{x/3})\ Ti^{4+}O_3 \qquad (4)$$

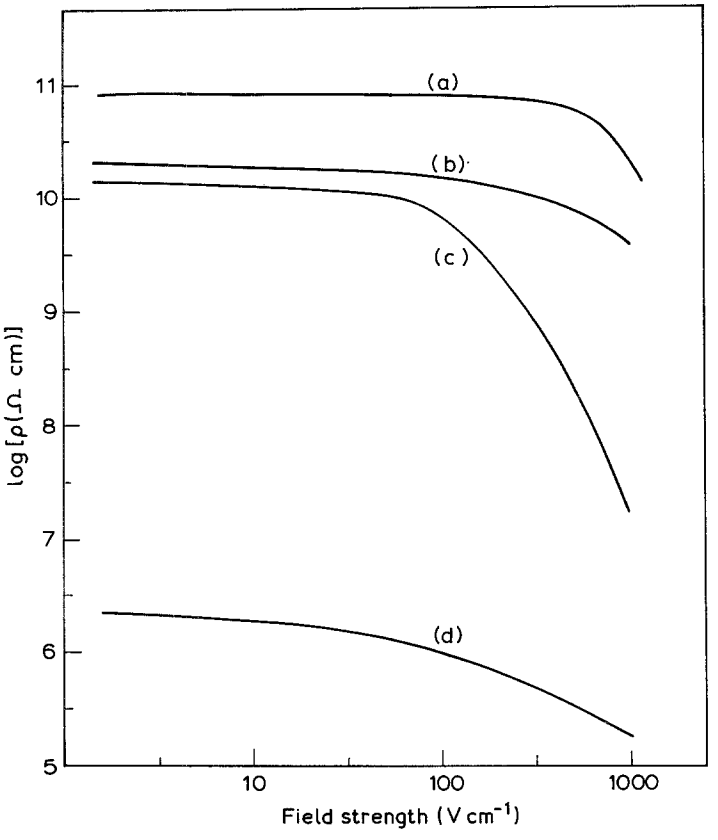

Figure 13 *I–V* characteristics for $(1 - x)BaTiO_3 + xNd_{2/3}TiO_3$ ceramics. (a) $x = 0.3$, (b) $x = 0.15$, slow cooling, 20 K h^{-1}, (c) $x = 0.15$, fast cooling, 200 K h^{-1}, (d) $x = 0.01$.

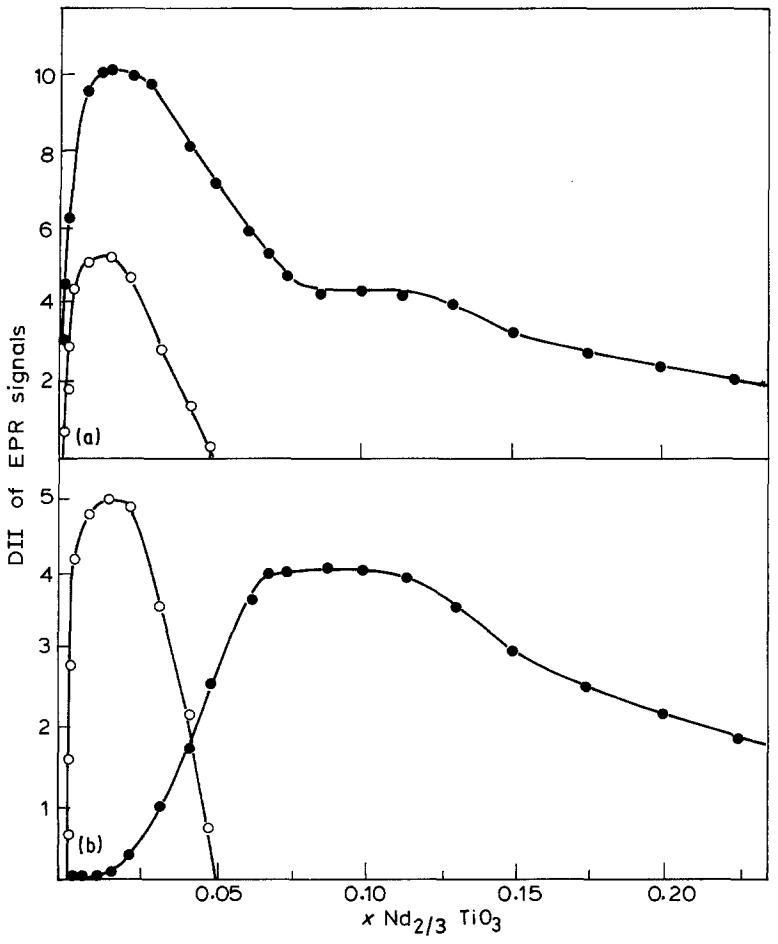

Figure 14 Variation of double-integrated intensities (DII) of (●) V'_{Ba}, $g = 1.997$ and (○) Ti^{3+}–V_O, $g = 1.963$ EPR signals with x-values in $(1 - x)BaTiO_3 + xNd_{2/3}TiO_3$ ceramics at (a) 400 and (b) 300 K.

However, cation vacancies at the titanium sublattice are also envisaged in a few of the recent publications [23, 24]. Alternatively, complex substitution at both barium and titanium sublattices is possible:

$$(Ba^{2+}_{1-x}Nd^{3+}_x)(Ti^{4+}_{1-x}Nd^{3+}_x)O_3 \qquad (5)$$

which requires neither electron nor cation vacancy compensations, thereby rendering the material insulating. Substitution of Ln^{3+} ions in the titanium sublattice is indicated from the luminescence and EPR studies on gadolinium- and europium-doped $BaTiO_3$ [25, 26].

An entirely different explanation for the enhancement of resistivity with neodymium content is the decreasing grain size as proposed by Wernicke [9, 27]. According to Wernicke the difference in the diffusion coefficient of V_{Ba} and V_O migrating from the grain boundary to the grain interior causes freezing-in of V_{Ba} around the grain boundary layers at low temperatures, since V_{Ba} is slow to equilibrate. However, the observations do not support this explanation for the following reasons: The grain size reaches a lower value of $x > 0.075$ (Fig. 8), whereas the cell parameters continue to decrease beyond this concentration (Fig. 1). Besides, the variations in the EPR intensities of Ti^{3+}–V_O and V'_{Ba} defect centres do not show any correlation with the change in grain size (Fig. 14). The persistence of the V'_{Ba} EPR signal ($g = 1.997$) in BNT ceramics with higher x-values indicates the prevalence of cation compensation in samples heavily substituted with neodymium. On the other hand, both electron and vacancy compensations prevail at low neodymium contents (Fig. 14). In previous publications [6, 7, 21, 22] we have shown that the acceptor states arising from barium vacancies are activated across the tetragonal-to-cubic phase transition and consequently trap electrons. Therefore the EPR signal arising from V'_{Ba} appears only in the cubic phase at $x < 0.075$. The decreasing intensity of the V'_{Ba} signal and the disappearance of the Ti^{3+}–V_O signal in the cubic phase at $x \sim 0.05$ are indicative of the change in compensation mechanism. Furthermore, the V'_{Ba} EPR signal is observed at 300 K for samples with $x > 0.0075$ due to the diffuse phase transition existing in this system [7]. At $x > 0.057$, $BaTiO_3$ is completely cubic at 300 K so that the EPR signal intensities of V'_{Ba} at 300 and 400 K are the same.

The X-ray powder patterns of BNT ceramics with $x < 0.3$ do not show any reflection other than those from cubic $BaTiO_3$. In contrast, the ED observations of samples with $x \geqslant 0.1$ indicate the presence of other phases which means that the additional phases are X-ray amorphous. Among these phases, the definitely identifiable one is $Nd_2Ti_2O_7$. The phase which shows broad ED rings must be amorphous (or glassy) and is produced by the solidification of a melt. Partial melting of BNT ceramics is evidenced from the DTA results. The lower X-ray intensities of $BaTiO_3$ in the sintered ceramics as when compared to those of $BaTiO_3 + Nd_2Ti_2O_7$ mixtures also support the presence of an amorphous phase. Thus the range of homogeneity in $(1 - x)BaTiO_3 + xNd_{2/3}TiO_3$ is limited to $x \leqslant 0.1$, though X-ray diffraction studies indicate $x \simeq 0.3$ as the homogenity limit. These

results are in contrast to the earlier literature on $BaTiO_3$ heavily doped with lanthanum, where a homogeneity range up to $x \simeq 0.3$ is envisaged [10, 15]. The decrease in the X-ray intensities of $BaTiO_3$ reflections unaccompanied by line-broadening, in conjunction with the DTA results, can be explained in terms of the dissolution of smaller $BaTiO_3$ grains to form a molten phase. Since BNT ceramics of $x > 0.15$ subjected to a longer duration of sintering acquire perceptible glaze and the SEM photographs of such specimens show solidification lineages, the amorphous phase may have a more glassy character around room temperature. This amorphous phase covers the $BaTiO_3$ grains as well as filling the triple points. Parallel changes can be envisaged in $Nd_2Ti_2O_7$ ceramics with increase in BaO content.

The above complexity arises from the limited solubility range and the absence of structural intergrowths in the $BaTiO_3$–$Nd_{2/3}TiO_3$ system. A series of compounds with the general formula $A_nTi_nO_{3n+2}$ ($n = 4, 5, \ldots$) is known for A = Ca (or Sr) + Ln, but not for barium. In the $CaTiO_3$–$Nd_2Ti_2O_7$ system, intergrowth of $Nd_2Ti_2O_7$ slabs within the perovskite matrix has been proposed [28, 29]. In systems involving $BaTiO_3$, increasing neodymium concentration gives rise to cubic perovskite with a high barium-vacancy concentration (Fig. 14). Since a larger cation vacancy content as a result of Nd^{3+} substitution cannot be accommodated in the $BaTiO_3$ lattice, the homogeneity limit is reached. This situation cannot be compared with that of La^{3+}-substituted Pb(Ti, Zr)O_3, where the deviation from stoichiometry gives rise to coupled defects in both lead and oxygen sublattices [30]. The larger non-stoichiometry leads to the formation of crystallographic shear planes, thus eliminating independent lead and oxygen vacancies [31, 32]. The absence of Ruddlesden–Popper-type phases in the $BaTiO_3$–BaO system is also a cause of restricted homogeneity. The new phases remain X-ray amorphous due to the partial melting behaviour of the BNT compositions, wherein $Nd_2Ti_2O_7$ crystallizes with increasing neodymium content. $BaTiO_3$ grains having rounded edges and corners (Fig. 6c) arise as a result of the partial dissolution in the melt and subsequent recrystallization.

The ε_{eff} values of BNT ceramics ($0.1 < x < 0.3$) are greater than those of conventional dielectric ceramics based on undoped $BaTiO_3$. The important dielectric characteristics, namely the grain-size dependence of ε_{eff}, the fall in ε_{eff} with the measuring frequency, the tan δ that goes through a minimum followed by enhancement at higher frequencies, the non-ohmic resistivities which obey a power-law relation with field-strength, the enhanced leakage current at higher applied field-strength accompanied by a decrease in ε_{eff} and rise in tan δ, are characteristics of intergranular (or grain-boundary) layer dielectrics [33]. In such ceramics, the intergranular behaviour is explained in terms of the conducting grain interiors that are surrounded by a highly resistive grain-boundary regions [6, 34–36]. The details of the microstructural dependence of the capacitance in such types of ceramic are discussed in these references. Generally, the effective capacitance between the electrodes can be expressed as

$$\varepsilon_{eff} = \varepsilon_0 \varepsilon_g (A/D)(d_g/d_s) \quad (6)$$

where ε_g is the dielectric constant of $BaTiO_3$, A is the area of the electrode, D is the thickness of the capacitor, d_g is the grain size and d_s is the thickness of the second-phase layer at the grain boundaries. The resistivity of the $BaTiO_3$ grain core will not be more than that of $BaTiO_3$ doped with 3.5 at % Nd ($x \simeq 0.0525$) (i.e. a cubic phase with no possible second-phase formation) which is $\sim 10^4$ to $10^6\,\Omega$ cm, whereas the resistivity of $Nd_2Ti_2O_7$ containing BaO is more than $10^{13}\,\Omega$ cm. The large difference in resistivity will bring about intergranular layer capacitance in BNT ceramics. Taking a typical value of $\varepsilon_{eff} \simeq 1.5 \times 10^4$ and that of cubic $BaTiO_3$ as about 1500, we obtain $D_g/d_s \sim 10$. Since d_g is about 2 μm, the average thickness of the grain boundary phase can be estimated as about 200 nm.

The interesting feature of BNT ceramics with $x > 0.1$ is their relative insensitivity to wider variations in chemical composition (Fig. 8). Besides, it is possible to prepare these dielectrics with more flexible processing conditions as compared to those of GBLCs with $x < 0.0075$ Nd [2–4]. This can be explained in terms of the grain-boundary model given in Fig. 15a. The intergranular material which separates the adjoining $BaTiO_3$–Nd grains has a variable thickness. The grain corners contain the bulk of the second phase, whereas it is thinner around the grain-to-grain contact points. In the thicker region, bulk conduction is through the insulating intergranular phase where the conductivity is low, so that the equivalent circuit can be as shown in Fig. 15b. In the thinner regions, the resistivity is lower so that the total reactive impedance has to be taken into consideration. Because the electrical paths of these small segments are parallel, a wider variation in neodymium content does not significantly alter the effective dielectric constant.

The presence of $Nd_2Ti_2O_7$ may lower the value of ε_{eff} since the compound has low ε values (ε(av) $\approx$ 40) over a wide temperature range. This may explain the lowering of ε_{eff} at higher x-values (Fig. 8). However, $Nd_2Ti_2O_7$ can effectively bring down the temperature coefficient of ε_{eff}, as can be expected from Lichtnecker's logarithmic rule of mixtures [37].

The general trends of increasing ε_{eff} above 350 K and the corresponding maximization of tan δ at low measuring frequencies are similar to those observed in relaxor ceramics such as bismuth-doped $SrTiO_3$ [38, 39]. This effect has been attributed to intrinsic ionic polarization enhanced by the distortion arising from the aliovalent donor ions in the crystal lattice. Different relaxing dipolar species such as impurities, lattice vacancies or second phases have been proposed in these materials. The dielectric behaviour can be alternatively explained in terms of the decrease in resistivity of grain cores with temperature, whereby the grain-core resistivity approaches the reactive impedance value of the grain-boundary phase. This may raise ε_{eff} as well as tan δ, particularly at low frequencies as discussed by Burn and Neirmann [36].

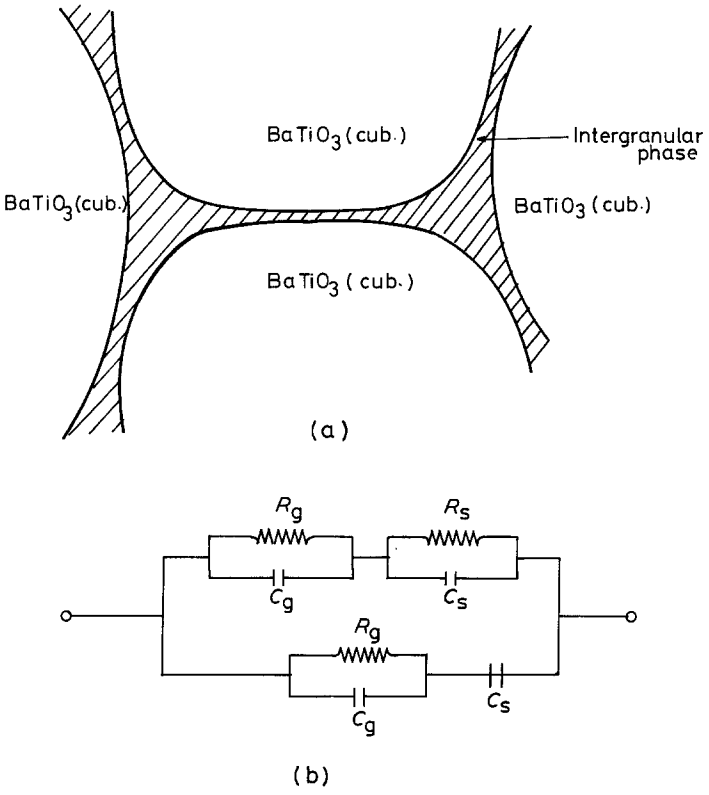

Figure 15 (a) Grain-boundary region in $(1 - x)$ $BaTiO_3 + xNd_{2/3}TiO_3$ ceramic with $0.15 < x < 0.225$. (b) Electrical equivalent circuit of the above region.

Acknowledgements

Thanks are due to CSIR, New Delhi for a research fellowship to P. Murugaraj.

References

1. O. SABURI, *J. Phys. Soc. Jpn* **14** (1959) 1159.
2. T. MURAKAMI, T. MIYASHITA, M. NAKAHARA and E. SEKINE, *J. Amer. Ceram. Soc.* **56** (1973) 294.
3. T. ASHIDA and H. TOYODA, *Jpn J. Appl. Phys.* **5** (1966) 269.
4. H. BRAUER, *Z. Angew. Phys.* **29** (1970) 282.
5. W. HEYWANG, *J. Mater. Sci.* **6** (1971) 1214.
6. P. MURUGARAJ and T. R. N. KUTTY, *Mater. Res. Bull.* **20** (1985) 1473.
7. P. MURUGARAJ, T. R. N. KUTTY and M. SUBBARAO, *J. Mater. Sci.* **21** (1986) 3521.
8. A. YAMAJI, Y. ENOMOTO, K. KINOSHITO and T. MURAKAMI, *J. Amer. Ceram. Soc.* **60** (1977) 97.
9. R. WERNICKE, *Phys. Status Solidi* **47** (1978) 139.
10. N. G. EROR and D. M. SMYTH, in "The chemistry of Extended Defects in Non-metallic Solids", edited by L. Eyring and M. O'Keefe (North-Holland, Amsterdam, 1970) p. 62.
11. S. R. RUDDLESDEN and P. POPPER, *Acta Crystallogr.* **11** (1958) 54.
12. U. BALACHANDRAN and N. G. EROR, *J. Amer. Ceram. Soc.* **64** (1981) C75.
13. T. Y. TIEN and F. A. HUMMEL, *Trans. Br. Ceram. Soc.* **66** (1967) 233.
14. D. HENNINGS, *Mater. Res. Bull.* **6** (1971) 321.
15. B. C. TOFIELD, *J. Solid State Chem.* **12** (1975) 270.
16. Y. H. HU, M. P. HARMER and D. M. SMYTH, *J. Amer. Ceram. Soc.* **68** (1985) 372.
17. L. G. SCHERBAKOVA, L. G. MAMSUROVA and G. E. SUKHANOVA, *Russ. Chem. Rev.* **48** (1979) 228.
18. D. KOLAR, Z. STADLER, S. GABERSECK and D. SUVOROV, *Ber. Deutsch, Keram. Ges.* **55** (1978) 346.
19. T. NEGAS, R. S. ROTH, H. S. PARKER and D. MINOR, *J. Solid State Chem.* **9** (1974) 297.
20. E. TILLMANNS, W. HOFMEISTER and W. H. BAUR, *ibid.* **58** (1985) 14.
21. T. R. N. KUTTY, P. MURUGARAJ and N. S. GAJBHIYE, *Mater. Lett.* **2** (5A) (1984) 396.
22. *Idem, Mater. Res. Bull.* **20** (1985) 565.
23. G. V. LEWIS, C. R. A. CATLOW and R. E. W. CASSELTON, *J. Amer. Ceram. Soc.* **68** (1985) 555.
24. H. M. CHAN, M. P. HARMER and D. M. SMYTH, *ibid.* **69** (1986) 507.
25. L. RIMAI and G. A. DeMARS, *Phys. Rev.* **127** (1962) 702.
26. S. MAKISHIMA, K. HOSEGAWA and S. SHIONOYA, *J. Phys. Chem. Solids* **20** (1962) 249.
27. J. DANIELS and R. WERNICKE, *Philips Res. Repts.* **31** (1976) 544.
28. R. PORTIER, M. FAYARD, A. CARPY and J. GALY, *Mater. Res. Bull.* **9** (1974) 371.
29. M. NANOT, F. QUEYROUX, J. C. GILLES, R. PORTIER and M. FAYARD, *ibid.* **10** (1975) 313.
30. D. HENNINGS and G. ROSENSTEIN, *ibid.* **7** (1972) 1505.
31. V. V. PRISEDSKY, V. P. KOMAROV, G. F. PANKO and V. V. KLIMOV, *Ferroelectrics* **23** (1980) 23.
32. A. H. MEITZLER, *ibid.* **11** (1976) 503.
33. R. M. GLAISTER, *Proc. IEE* **109 B** (Suppl. 22) (1961) 423.
34. S. WAKU, N. NISHIMURA, T. MURAKAMI, A. YAMAJI, T. EDAHIRO and M. UCHIDATE, *Rev. Elect. Commun. Lab.* **19** (1971) 665.
35. R. WERNICKE, in "Advances in Ceramics", edited by L. M. Levinson, (American Ceramic Society, Ohio, 1981) p. 272.
36. I. BURN and S. NEIRMAN, *J. Mater. Sci.* **17** (1982) 3510.
37. K. LICHTNECKER, *Phys. Z.* **27** (1926) 115.
38. G. I. SKANAVI and E. N. MATVEEVA, *J. Exp. Theor. Phys.* **30** (1956) 1049.
39. L. E. GOSS, *Proc. IEE* **109B** (Suppl. 22) (1961) 407.

Received 11 November 1986
and accepted 11 February 1987